



Published in final edited form as:

*J Am Chem Soc.* 2019 July 10; 141(27): 10777–10787. doi:10.1021/jacs.9b04303.

## Transition State Asymmetry in C–H Bond Cleavage by Proton-Coupled Electron Transfer

Julia W. Darcy<sup>†</sup>, Scott S. Kolmar<sup>†</sup>, James M. Mayer<sup>\*</sup>

Department of Chemistry, Yale University, New Haven, Connecticut 06520-8107, United States

### Abstract

The selective transformation of C–H bonds is a longstanding challenge in modern chemistry. A recent report details C–H oxidation via multiple-site concerted proton–electron transfer (MS-CPET), where the proton and electron in the C–H bond are transferred to separate sites. Reactivity at a specific C–H bond was achieved by appropriate positioning of an internal benzoate base. Here, we extend that report to reactions of a series of molecules with differently substituted fluorenyl-benzoates and varying outer-sphere oxidants. These results probe the fundamental rate versus driving force relationships in this MS-CPET reaction at carbon by separately modulating the driving force for the proton and electron transfer components. The rate constants depend strongly on the  $pK_a$  of the internal base, but depend much less on the nature of the outer-sphere oxidant. These observations suggest that the transition states for these reactions are imbalanced. Density functional theory (DFT) was used to generate an internal reaction coordinate, which qualitatively reproduced the experimental observation of a transition state imbalance. Thus, in this system, homolytic C–H bond cleavage involves concerted but asynchronous transfer of the  $H^+$  and  $e^-$ . The nature of this transfer has implications for synthetic methodology and biological systems.

### Graphical Abstract

---

<sup>\*</sup>Corresponding Author: james.mayer@yale.edu.

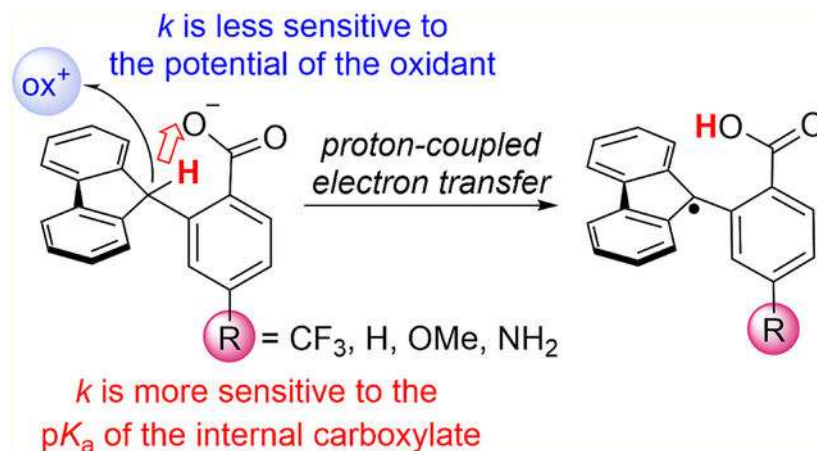
<sup>†</sup>J.W.D. and S.S.K. contributed equally to this work.

#### Supporting Information

The Supporting Information is available free of charge on the ACS Publications website at DOI: 10.1021/jacs.9b04303.

Synthesis and characterization, kinetic procedures and tabulated data, DFT calculations, and DFT calculated coordinates (PDF)

The authors declare no competing financial interest.



## INTRODUCTION

The selective transformation of C–H bonds remains one of the primary challenges facing modern chemistry. The practical and fundamental interest in manipulating these inert bonds has stimulated decades of research from the organometallic, synthetic, biological, inorganic, and physical organic chemistry communities.<sup>1</sup> Many methods have been developed to overcome the inertness of C–H bonds, including the use of activating and directing groups, selective catalysts, and supramolecular recognition.

Hydrogen atom transfer (HAT) is the classical mechanism for C–H bond activation, central to combustion, free-radical halogenation, and many other processes.<sup>2</sup> HAT is one kind of proton-coupled electron transfer (PCET) process, in which a hydrogen atom, a proton and electron ( $H^+ + e^- \equiv H^\bullet$ ), is transferred from one group to another in a single kinetic step.<sup>3</sup> HAT mechanisms for C–H bond activation have a strong intrinsic selectivity and can be harnessed in a number of ways for processes from petrochemical scale to synthetic organic transformations.<sup>2e,4</sup>

Most enzymatic oxidations of unactivated C–H bonds are described as HAT processes, including heme and nonheme iron and copper enzymes.<sup>5</sup> Many of these and other biological reactions, however, might be better described as multiple-site concerted proton–electron transfer (MS-CPET). MS-CPET reactions occur when electrons and protons are transferred to or from disparate sites or cofactors.<sup>3</sup> In cytochrome P450 oxidations, for example, C–H bonds are cleaved by proton transfer to the oxo group concerted with electron transfer to a heme/thiolate-based orbital.<sup>6</sup> HAT and MS-CPET are widely utilized, from biological to energy to synthetic processes, as the concerted transfer of protons and electrons can avoid high energy, charged intermediates.<sup>7</sup>

Well-characterized examples of MS-CPET, in both synthetic and biological contexts, have occurred nearly exclusively at polar bonds, typically at O–H or N–H bonds. In these systems, MS-CPET proceeds through the preformation of a hydrogen bond, which serves to align the proton transfer coordinate.<sup>8</sup> The canonical biological example of MS-CPET is the oxidation of TyrZ in photosystem II, where the phenolic bond is cleaved by proton transfer

to a proximal histidine ligand accompanied by long-range electron transfer to  $P_{680}^{+9}$ . Similarly, MS-CPET reactions in small-molecule model systems<sup>10</sup> and synthesis reactions<sup>11</sup> all occur at polar bonds.

We recently demonstrated that MS-CPET can occur directly at the C–H bond in the absence of classical hydrogen-bonding interactions.<sup>12</sup> In the fluorenyl-benzoate shown in Scheme 1, Flr(H)CO<sub>2</sub><sup>−</sup>, the fluorenyl C–H bond is oxidized by proton transfer to an internal carboxylate concerted with electron transfer to an outer-sphere oxidant (Scheme 1). Use of MS-CPET as a strategy for activating C–H bonds relies on the appropriate positioning of a basic cofactor to provide the necessary kinetic setting for proton transfer.<sup>12</sup>

Our previous report examined the variation in the rate constant for oxidation of Flr(H)CO<sub>2</sub><sup>−</sup> with various outer-sphere oxidants. The rate versus driving force relationship upon changing the oxidant was found to be very shallow:  $\partial \ln(k)/\partial \ln(K_{eq}) = \partial \Delta G^\ddagger/\partial \Delta G^\circ = \alpha = 0.2$ . Semiclassical Marcus-theory type treatments predict an  $\alpha$  of 0.5, and this is what has typically been observed in both HAT and MS-CPET reactions.<sup>2a,3,13</sup> The small  $\alpha$  shows that the reaction rate constants are not greatly affected by the nature of the outer-sphere oxidant.

We hypothesized that the shallow dependence on the potential of the oxidant could be due to an asynchronous or imbalanced transition state. Transition state imbalances have been extensively described for E2 elimination reactions<sup>14</sup> and deprotonation of nitroalkanes,<sup>15</sup> and have been observed in many classes of bond breaking and forming reactions.<sup>16</sup> Jencks invoked imbalanced transition states in describing structure–reactivity coefficients in the 1970s; these ideas were developed into the widely used visualizations presented in More O’Ferrall–Jencks plots.<sup>17</sup> Building on this framework, Bernasconi introduced his Principle of Nonperfect Synchronization (PNS) to describe elementary reactions that involve multiple concurrent processes, for example, bond formation/ cleavage and electronic localization/ delocalization. Differences in the progression of these processes at the transition state are called imbalances.<sup>16,18</sup> Complementary multidimensional analyses have been developed by Grunwald<sup>19</sup> and Guthrie.<sup>20</sup> Asynchronicity has very recently been discussed for metal-mediated HAT reactions of C–H bonds, which can occur through multiple mechanisms.<sup>21</sup> Asynchronicity is important from a practical perspective because when different thermochemical parameters affect transition state energetics differently, rates and selectivities can be modulated by the choice of reagents.

The fluorenyl-benzoate system (Flr(R)CO<sub>2</sub><sup>−</sup>) is an ideal model to study fundamental aspects of MS-CPET at C–H bonds. Herein, we demonstrate that independently modulating the proton transfer and electron transfer portions of the reaction result in very different rate versus driving force relationships (Scheme 1). The observed discrepancies in the rate/driving force relationships suggest an imbalanced or asynchronous transition state, where electronic reorganization and proton transfer have occurred to different extents. Density functional theory (DFT) methods were used to contextualize the experimental results and were analyzed in the context of Bernasconi’s PNS. Overall, the results inform how the rate of C–H bond oxidation can be controlled by changes to the electron or proton transfer reaction coordinates, and suggest how selectivity could be achieved in synthetic and biological contexts.

## RESULTS

### Synthesis/Characterization.

The compounds shown in Scheme 1 were synthesized via a Pd-catalyzed coupling reaction between fluorene and the corresponding para-substituted methyl 2-bromobenzoate in DMF.<sup>22</sup> The carboxylic acid derivatives Flr(R)CO<sub>2</sub>H were obtained from the respective methyl esters via base hydrolysis (see Supporting Information section 2 for details).

The carboxylic acids were deprotonated in situ using a slightly substoichiometric amount of tetrabutylammonium hydroxide (TBAOH, as a 1 M solution in MeOH). Oxidation reactions of the carboxylates were performed with various para-substituted aminium (NAr<sub>X</sub><sup>•+</sup>) and ferrocenium (Fc<sup>+</sup>) oxidants. The driving force for reactions with this series of oxidants spans 1.2 V. Oxidations of the carboxylates each gave good yields of the corresponding lactone with regeneration of protonated starting material, as described previously for the R = H derivative (see the Supporting Information).<sup>12</sup>

### Kinetics of Oxidation Reactions.

The kinetics of oxidation were measured for all four carboxylates with up to seven different aminium and ferrocenium oxidants in MeCN solvent (Figure 1A, Table 1). The carboxylate was generated in situ immediately before the reaction by deprotonating with 0.9 equiv of tetrabutylammonium hydroxide (TBAOH, as a solution in MeOH). Reactions were performed with an excess of carboxylate relative to the oxidant (3–30 equiv). The time-courses of the oxidations were monitored optically using a stopped-flow instrument, following the disappearance of the colored oxidants (Figure 1B). Each full set of absorbance spectra over time was fit using SpecFit global-fitting software.<sup>23</sup> The rate constant for the C–H bond oxidation step,  $k_{\text{MS-CPET}}$ , is one-half of the measured rate constants ( $k_2$  in Table 1) because 2 equiv of the oxidant is consumed in the total reaction, although the MS-CPET step is rate-limiting.<sup>12</sup> The data for the R = H compound ( $\alpha_{\text{ET}}(\text{H})$  line in Figure 1C) were reported in our previous study.<sup>12</sup>

Reactions of the carboxylates with the oxidants fit well to a second-order kinetic model, with a few exceptions. Reactions of both the NH<sub>2</sub>- and the CF<sub>3</sub>-derivatives with the stronger aminium oxidants (e.g., N(Ar<sub>OMe</sub>)(Ar<sub>Br</sub>)<sub>2</sub><sup>•+</sup>) display deviations from the second-order model, likely due to oxidant/base incompatibilities.<sup>24</sup> The most electron-rich and the most electron-poor of these series of benzoates have undesirable side reactions that occur with stronger oxidants (Supporting Information section 3). These incompatibilities can be mitigated by using the weaker ferrocenium oxidants, as these are less susceptible to nucleophilic attack by the carboxylate, for example.

Bimolecular rate constants for the reactions of Flr(OMe)CO<sub>2</sub><sup>-</sup>, Flr(H)CO<sub>2</sub><sup>-</sup>, and Flr(CF<sub>3</sub>)CO<sub>2</sub><sup>-</sup> with N<sup>•+</sup>(Ar<sub>OMe</sub>)<sub>3</sub> were measured at different temperatures. Using data from –40 to 15 °C for the first two compounds, and from –20 to 15 °C for the CF<sub>3</sub> derivative, the Eyring parameters in Table 2 were obtained (Supporting Information section 3.4). The data show that the free energies of activation are enthalpy controlled.

### Thermochemical Analysis.

The driving forces for the various C–H bond oxidation reactions were determined using the thermochemical cycle in Scheme 2. The relative  $pK_a$ 's of Flr(R)CO<sub>2</sub>H in MeCN (eq 2) were determined experimentally by equilibration of each carboxylate with 4-trifluoromethylbenzoic acid (TFBA) and monitoring by <sup>1</sup>H and <sup>19</sup>F NMR spectroscopies in CD<sub>3</sub>CN, using a previously described method.<sup>10d</sup> Absolute values were determined by equilibrating TFBA with benzoic acid ( $pK_a = 21.5$ ).<sup>25</sup> The experimental  $pK_a$ 's vary over a range of 1.7 units (Table 3). While the MS-CPET processes should initially form the *E*-isomers of the carboxylic acids, not the more stable *Z*-forms, the relative energetics of these isomers varies only slightly with substituents (based on computational studies).<sup>26</sup> Thus, the differences in the measured  $pK_a$  values should be sufficient for the relative MS-CPET free energy calculation in Scheme 2.

The relative C–H bond dissociation free energies (BDFEs, eq 1) for Flr(R)CO<sub>2</sub><sup>−</sup> and Flr(R)CO<sub>2</sub>H were determined computationally, as described below (see also Supporting Information section 4.1). The reaction being studied involves cleavage of the C–H bond in the carboxylate form (Figure 1A), so those values are used in the Discussion and are in Table 3. However, the thermochemical cycle to determine the overall driving force uses the  $BDFE_{CH}(CO_2H)$  for the carboxylic acid because that allows the use of the experimental  $pK_a$  values (Scheme 2) (Supporting Information section 4.1). The free energy to separate H<sup>•</sup> into e<sup>−</sup> and H<sup>+</sup> (eq 3) is constant over the series,<sup>7</sup> and the reduction potentials of the oxidants (eq 4) were taken from previous reports.<sup>10d,27</sup>

The relative bond dissociation free energies of the fluorenyl C–H bond ( $\Delta BDFE_{CH}$ ) for the carboxylate with different R substituents were computed using Density Functional Theory (DFT). The computations used B3LYP/def2-TZVP with a polarized continuum model (PCM) in acetonitrile solvent. Free energies were calculated for isodesmic reactions between the carbon radical of one carboxylate species and the C–H bond of a second carboxylate compound (Supporting Information section 4.2). The change in BDFE with substituent is given in Table 3 relative to the R = H compound. The  $BDFE_{CH}(CO_2^-)$  changes by less than 1 kcal mol<sup>−1</sup> with changes to R, presumably because the substituents are meta to the radical center.<sup>28</sup>

### Rate versus Driving Force Relationships.

The values in Table 3 and the analysis in Scheme 2 give the relative free energies (eq 6) and equilibrium constants,  $\Delta \log(K_{eq}) = -\Delta \Delta G^\circ / 2.303RT$ , for all of the C–H bond cleavage reactions. The rate constants can be compared to the  $\Delta \log(K_{eq})$  values to examine rate versus driving force linear free energy relationships (LFERs). The full set of rate versus driving force data for the four derivatives studied, with various oxidants, is shown in Figure 1C. Most sets of single-step reactions such as those studied here follow a single linear free energy relationship (LFER), such as eq 7.<sup>17c</sup> The slope of this relationship  $\alpha$  indicates how the logarithm of the rate constant changes with a given change in  $\Delta \log(K_{eq})$ .

$$\Delta \Delta G_{rxn}^\circ = \Delta BDFE_{CH}(CO_2H) - 1.37 \Delta pK_a - 23.06 E_{OX} \quad (6)$$

$$\Delta\log(k_{\text{MS-CPET}}) = \alpha\Delta\log(K_{\text{eq}}) \quad (7)$$

The data set in Figure 1C is interesting because the dependence of  $\log(k_{\text{MS-CPET}})$  on  $\Delta\log(K_{\text{eq}})$  cannot be fit by a single LFER. Even though the compounds and reactions are very similar, a given value of  $\Delta\log(K_{\text{eq}})$  corresponds to four different  $\log(k_{\text{MS-CPET}})$  values, for the four different substrates. The four MS-CPET rate constants at the same  $\Delta\log(K_{\text{eq}})$  differ by almost 2 orders of magnitude.

Two different sets of LFERs are needed to describe the results. The dependence of  $\log(k_{\text{MS-CPET}})$  on  $\Delta\log(K_{\text{eq}})$  for a single substrate over a series of oxidants will be termed the electron transfer  $\alpha$ ,  $\alpha_{\text{ET}}$ , because the  $K_{\text{eq}}$  is changed only by using outer-sphere oxidants with different reduction potentials. The  $\alpha_{\text{ET}}$  value reports on how the rate constants respond to changes in the electron transfer component of MS-CPET. As shown in Figure 1C, all of the substrates have  $\alpha_{\text{ET}} \cong 0.2$ , as found for Flr(H)CO<sub>2</sub><sup>-</sup> in our previous report.<sup>12</sup> The rate constants are much larger for the substrates with the more basic carboxylates; for instance, the rate constants for the -NH<sub>2</sub> compound are on average an order of magnitude larger than those for -OMe.

The LFERs for reactions of a single oxidant with the four differently substituted compounds have much steeper slopes. This is shown in Figure 1C by the box surrounding the four data points for reactions with Fe<sup>+</sup>. These four points are plotted in Figure 1D and show a slope of 0.58. We term this the Brønsted  $\alpha_{\text{Fc}^+}$ , to indicate that it reflects changes in the reactivity of the R-substituted fluorenes with Fe<sup>+</sup>. For five of the seven different oxidants studied, the Brønsted  $\alpha_{\text{ox}^+}$  values are within the uncertainty of this 0.58 value (0.48–0.61); N(Ar<sub>OMe</sub>)<sub>2</sub> (Ar<sub>Br</sub>)<sup>+</sup> (0.36) and Br FeCp\*<sub>2</sub><sup>+</sup> (0.99) are a bit different (Supporting Information section 3.3, uncertainties  $\sim \pm 0.1$ ). All of the  $\alpha_{\text{ox}^+}$  values are substantially larger than the  $\alpha_{\text{ET}}$  for changes in the oxidant with a given substituted compound (2–5 times larger).

The rate constants are much more sensitive to changes in  $K_{\text{eq}}$  that result from changing the benzoate substituent versus changes in  $K_{\text{eq}}$  from different outer-sphere oxidants (Figure 1C vs D). In the set of oxidations by FeCp<sub>2</sub><sup>+</sup>, for instance, the rate constant for Flr(NH<sub>2</sub>)CO<sub>2</sub><sup>-</sup> is 270 times faster than that of Flr(CF<sub>3</sub>)CO<sub>2</sub><sup>-</sup> for a difference in the equilibrium constants of 10<sup>4</sup> (Figure 1D). In contrast, changing the oxidant from FeCp<sub>2</sub><sup>+</sup> to FeCp\*<sub>2</sub><sup>+</sup>, a change in  $K_{\text{eq}}$  of  $3.5 \times 10^4$  results in a change in  $k_{\text{MS-CPET}}$  of only a factor of 5. These data highlight the large difference in slope between these two LFERs.

### DFT Calculated Potential Energy Surfaces.

A computational investigation was undertaken to understand the origin of the very different dependencies on changing the oxidant versus changing the substituent in these MS-CPET reactions. In particular, we aimed to understand what features of the reaction coordinate might account for this distinction. To do this, we have calculated the internal reaction coordinate (IRC). This is defined as the minimum energy reaction pathway that connects a transition state (TS) to the reactants and products of a reaction. We take the IRC to be a reasonable description of the potential energy surface (PES).

Our approach to analyzing these reactions follows the computational studies of PT at carbon centers by Bernasconi.<sup>29</sup> While such adiabatic DFT calculations are not the best approach to a reaction with an outer-sphere electron transfer component, we believe that this side-by-side comparison of PT and MS-CPET provides valuable insights. There are much more sophisticated theoretical treatments of proton-coupled electron transfer reactions.<sup>30</sup> In particular, Sayfutyarova, Goldsmith, and Hammes-Schiffer have very recently reported a study of the oxidations of  $\text{Flr(H)CO}_2^-$  that treats the proton as a quantum particle and emphasizes the importance of vibrational excited states.<sup>31</sup>

Our goal with these DFT studies was to connect with the prior physical-organic literature on proton transfers from C–H bonds and its emphasis on imbalanced transition states. To that end, we first describe computations of the intramolecular proton transfer (PT) from the fluorenyl C–H to the carboxylate in  $\text{Flr(H)CO}_2^-$ . We then use the same methodology to explore the more complicated MS-CPET reactions between  $\text{Flr(H)CO}_2^-$  and  $\text{N(Ar}_B)_3^{*+}$  and  $\text{N(Ar}_H)_3^{*+}$ .

The IRCs for intramolecular PT and MS-CPET were calculated using B3LYP/def2-SVP, because the MS-CPET calculation with the def2-TZVP basis set was prohibitively expensive. Both used a PCM solvent model with acetonitrile solvent. First, the geometries of the substrate and the product were optimized. Best guess structures for the TS then were used as a starting point for transition state calculations. The true TS structures (at this level of theory) were identified (i) by having a single imaginary frequency along the appropriate reaction coordinate (proton transfer between the fluorenyl carbon and the carboxylate oxygen) and (ii) by IRC calculations of the minimum energy pathway giving the optimized reactant and products (Supporting Information sections 4.2, 4.3, and 4.5). The degree of proton transfer and electronic reorganization (vide infra) were then quantified along the IRC and at the TS.

For both PT and MS-CPET, progress along the proton transfer coordinate was defined as the distance between the fluorenyl proton and carboxylate oxygen. For MS-CPET, the extent of electron transfer was determined from the change in the natural bond orbital (NBO) charge on the nitrogen atom of the oxidant. Although the charge is delocalized into the phenyl rings of the oxidant, the nitrogen atom undergoes the largest change in charge and thus provides a good measure of electron transfer.

The calculations were also used to indicate the progress of the Bernasconi-type “electronic reorganization” within the fluorenyl group along this reaction coordinate.<sup>32</sup> We chose to use the pyramidalization of the fluorenyl carbon as a measure of this reorganization, because it reflects the extent of rehybridization from the starting saturated  $\text{sp}^3$  center to the  $\text{sp}^2$  carbanion or radical product of PT or MS-CPET, respectively. This choice follows Bernasconi’s calculations of the deprotonation of acetaldehyde showing that pyramidalization of the  $\alpha$ -carbon lags significantly behind proton transfer to form the enolate.<sup>18c,29a</sup> In our analysis, the sum of the CCC bond angles around the fluorenyl carbon showed the progress as it varied from  $338^\circ$  in the  $\text{sp}^3$  reactant to  $358^\circ$  in the  $\text{sp}^2$  products.

For intramolecular proton transfer in  $\text{Flr(H)CO}_2^-$ , PT is computed to be endoergic, with  $\Delta E = +5.8 \text{ kcal mol}^{-1}$  and  $\Delta G^\circ = +6.5 \text{ kcal mol}^{-1}$  (Figure 2). The highest energy point along the IRC, the TS, occurs when the proton transfer has made 76% progress toward the product. At this point, analysis of the TS structure shows that the sum of the fluorenyl CCC bond angles is  $349^\circ$ , which is only 45% progress toward the planar product (Figure 2C and E). This indicates that for the PT reaction, PT is ahead of fluorenyl rehybridization, or electronic reorganization. This observation has been made for many other deprotonation reactions at carbon, as discussed below.

In comparison, the potential energy surface for MS-CPET between  $\text{Flr(H)CO}_2^-$  and  $\text{N(Ar}_{\text{Br}})_3^{*+}$  is highly exoergic, with  $\Delta E = -17 \text{ kcal mol}^{-1}$  and  $\Delta G^\circ = -20.5 \text{ kcal mol}^{-1}$ , and has a small barrier. The NBO charge on the nitrogen atom of the oxidant stays constant until the TS, then abruptly becomes more positive and stays constant for the remainder of the reaction (Supporting Information section 4.3). Thus, at this level of theory, the ET component of the reaction occurs at the TS. At the TS, the proton transfer has made 44% progress toward the product, while the sum of the fluorenyl CCC bond angles is  $344^\circ$ , only 29% progress toward the product (Figure 2D and F). As in the computations of the PT reactions, the TS shows greater progress in PT than in the electronic rearrangement of the fluorenyl group. A similar result was found for the  $2.1 \text{ kcal mol}^{-1}$  less exoergic MS-CPET reaction of  $\text{Flr(H)CO}_2^-$  with  $\text{N(Ar}_{\text{H}})_3^{*+}$  (Supporting Information section 4.5). (Calculations with ferrocenium oxidants were found to be too computationally expensive.) As expected from Hammond's postulate, the less exoergic reaction has proceeded farther along the reaction coordinate, but the asymmetry is still observed. In this case, PT has made 50% progress toward the product, while the sum of the fluorenyl CCC bond angles has made only 31% progress toward the product.

Both the MS-CPET and the PT reactions proceed with significantly more proton transfer from the C–H bond than electronic reorganization within the fluorenyl group. In both cases, electronic reorganization lags far behind the proton transfer at the transition state. In the MS-CPET cases, it is striking that, despite the strongly exoergic nature of the reaction, the proton has moved roughly halfway along its coordinate.

## DISCUSSION

Presented here is a detailed kinetic study of the factors that affect the cleavage of the C–H bond in four fluorenyl-benzoate compounds by multiple-site concerted proton–electron transfer (MS-CPET). As emphasized in our initial study of the oxidation of the  $\text{R} = \text{H}$  compound, these reactions proceed via concerted transfer of  $e^-$  and  $\text{H}^+$  because the alternative initial PT or initial ET steps are highly unfavorable.<sup>12</sup> The data presented herein show that the rates of this reaction are very sensitive to substituents *para* to the benzoate base, but quite insensitive to the reduction potential of the outer-sphere oxidant.

The dependence of the rate constants on driving force for this series of similar MS-CPET reactions cannot be described by a single linear free energy relationship (LFER). There is not a one-to-one correspondence of  $\log(k_{\text{MS-CPET}})$  with the changes in the free energies of the reaction, described by  $\Delta\log(K_{\text{MS-CPET}})$ . LFERs of very different slopes are observed,



depending on whether the driving force is changed via changes in the outer-sphere oxidant or the benzoate substituent (Figure 1C vs D).

Traditionally, experimental studies of MS-CPET (and other types of PCET reactions) have used a Marcus theory approach.<sup>3</sup> Most PCET reactions that have been studied at this level of detail show sensitivities similar to those of ET and PT driving forces and  $\alpha$ 's close to 0.5.<sup>10a,d,33,34</sup> We have argued that such results imply synchronous transfer of the  $e^-$  and  $H^+$ , with balanced transition states. A recent study by the Knowles group of ketone reductions found a shallow  $\alpha$ , with the rate constants responding equally to changes in the PT and ET portions.<sup>35</sup> These reactions therefore proceed via synchronous PCET. Goetz and Anderson recently reported HAT reactions that are more dependent on the  $pK_a$  of the substrate than the C-H BDFE.<sup>21b</sup> There are also PCET reactions that do not show simple correlations of rate with driving force.<sup>36</sup>

The results reported here do not fit a simple Marcus-type model. The observation that  $k_{MS-CPET}$  does not simply correlate with  $\Delta G^\circ_{MS-CPET}$ , the presence of two LFERs for the same range of driving forces, would require that the intrinsic barriers vary substantially with substituent. This seems very unlikely given the similarity of the compounds and because the same  $\alpha_{ET}$  is seen for each compound.

There are a number of other possible approaches that could be used to interpret the apparent dual dependence of  $\log(k_{MS-CPET})$  on  $\log(K_{eq-MS-CPET})$ . A very recent study of Sayfutyarova, Goldsmith, and Hammes-Schiffer analyzed the oxidation of  $Flr(H)CO_2^-$  with an approach that includes the quantum mechanical nature of the transferring proton.<sup>31</sup> They found significant contributions from vibrational excited states in the reactant and product.

In this study, we have chosen to use an adiabatic DFT model with a classical proton. While this cannot capture some effects, it allows a direct comparison with classical physical-organic studies of proton transfer from C-H bonds. In this model, the discrepancy between the LFERs suggests that the  $H^+$  and  $e^-$  transfer in a concerted but asynchronous manner. DFT calculations indicate that proton transfer is much more advanced at the transition state than electronic reorganization, as observed in many proton transfer reactions at carbon.<sup>16,32,37</sup> In this Discussion, we identify the dominant effect of the substituents and then contextualize the results in terms of precedent in the physical organic chemistry literature. The strong analogies found between PT and MS-CPET at C-H bonds are an important conclusion of this study.

### Disentangling Substituent Effects.

Varying the outer-sphere oxidant has the same effect for each of the four compounds (Figure 1C): the rate constants show a shallow dependence on the change in the equilibrium constant. The  $\alpha_{ET}$ , defined as  $\Delta\log(k_{MS-CPET})/\Delta\log(K_{eq})$ , is 0.2 in all four cases. Analysis of the effects of the different substituents is more complicated, however, because the changes in substituent affect multiple properties of the fluorenyl-benzoate molecules.

Our analysis takes the following conceptual approach. We consider that the fluorenyl radical is formed by homolytic cleavage of the C-H bond, with the proton and electron formed by

this cleavage being transferred to the carboxylate and the oxidant, respectively. This approach is related to Savéant's theory of electron transfer concerted with bond cleavage, which emphasizes the strength of the bond being cleaved, for example, in electrochemical carbon-halogen and peroxide O–O bond cleavages.<sup>38,39</sup>

For the Flr(R)CO<sub>2</sub><sup>−</sup> compounds, changing the R-group affects both the basicity of the carboxylate and the C–H BDFE. The larger effect is on the basicity, which experimentally shifts by 1.7 pK<sub>a</sub> units, corresponding to a change in ΔG° of 2.3 kcal mol<sup>−1</sup>. Shifts also occur in the ΔBDFE<sub>C–H</sub>'s for the fluorenyl C–H bonds in Flr(R)CO<sub>2</sub><sup>−</sup>, computed to vary by 0.9 kcal mol<sup>−1</sup> (Table 2). The CF<sub>3</sub> compound has the strongest C–H bond and is the slowest-reacting substrate. However, the pattern of reactivity does not otherwise follow the small changes in computed ΔBDFEs. Additionally, the –OMe compound reacts 3 times faster than even the R = H compound, although the R = OMe is computed to have a slightly stronger C–H bond. While these comparisons may approach the limit of relative computational accuracy, the changes in the C–H BDFEs with benzoate substituent do not appear to be the major contributor to the large variation of k<sub>MS-CPET</sub> with substituent.

The data indicate that the effects of the benzoate substituents are primarily based on changes in the basicity of the carboxylate acceptor. The spacing of the LFER lines in Figure 1C, for instance, generally echoes differences in experimental pK<sub>a</sub> values for Flr(R)CO<sub>2</sub>H (ΔpK<sub>a,COOH</sub>, Table 2), within the accuracy of the measurements. The large Brønsted α<sub>ox+</sub> values thus suggest a great sensitivity to the strength of the base, and to the proton transfer portion of the MS-CPET reaction.

### Imbalanced Transition States.

The computed proton potential energy surfaces for the MS-CPET reactions described above suggest imbalanced transition states for the MS-CPET reactions. In particular, proton transfer appears to be more advanced than expected from a simple Hammond postulate analysis. Even though the reactions of Flr(H)CO<sub>2</sub><sup>−</sup> and N(Ar<sub>Br</sub>)<sub>3</sub><sup>•+</sup> or N(Ar<sub>H</sub>)<sub>3</sub><sup>•+</sup> are strongly exoergic, at the TS the proton transfer has progressed roughly halfway to the product. PT is more advanced than the electronic reorganization within the fluorenyl unit to accommodate the incipient radical (for MS-CPET) or carbanion (for simple PT). The calculations are consistent with the experimental observation of two Brønsted α values. In many cases, the Brønsted α is taken as a rough measure of the transition state position.<sup>17c,40</sup> The larger α<sub>ox+</sub> values for changes in substituents should therefore imply a transition state that is later, more product like, along the proton transfer coordinate. We believe that these analyses provide a qualitative rationale for the high sensitivity of our MS-CPET reactions to the basicity of the carboxylate.

Reactions with imbalanced transition states have long been discussed in the physical organic literature. In particular, Bernasconi has argued that this is a very common situation, as enunciated in his Principle of Nonperfect Synchronization (PNS).<sup>18a,b,c,29a,b,41</sup> Others have developed similar ideas in different formalisms, including Marcus,<sup>42</sup> Kresge,<sup>15,40</sup> More O'Ferrall, Jencks, Grunwald, Guthrie,<sup>19,20,43</sup> and Bordwell.<sup>15</sup> One classic example is the deprotonation of nitroalkanes, where C–H bond cleavage is more pronounced at the TS than the electronic delocalization of the π system.<sup>15,37d</sup>

The DFT analysis shows that pure proton transfer in  $\text{Flr(H)CO}_2^-$  behaves similarly to traditional C–H bond deprotonations, for example, in aldehydes or nitroalkanes.<sup>16,18c</sup> The  $\text{Flr(H)CO}_2^-$  PT transition state is imbalanced, with proton transfer being farther along than the electronic reorganization within the fluorene, as indicated by the planarization of the incipient radical.

The imbalance of the proton transfer in  $\text{Flr(H)CO}_2^-$  is illustrated in Figure 3A by a traditional More O’Ferrall–Jencks plot.<sup>17a,44</sup> The horizontal axis represents progress along the PT coordinate, and the vertical axis represents progress along the internal electronic reorganization coordinate. A synchronous reaction would be indicated by progress along the diagonal of the square. The asynchrony of PT in  $\text{Flr(H)CO}_2^-$  is indicated by the curved line that connects the reactant to the product (bottom left to top right corners). Because the transition state has more progress along the proton transfer coordinate than the electronic reorganization coordinate, the lines are curved toward the bottom right corner.

Extending Bernasconi’s PNS to MS-CPET requires thinking not only about proton transfer and electronic reorganization but also about the electron transfer portion of the reaction. The adiabatic DFT calculations used here are not the preferred treatment for electron transfer processes, which can be nonadiabatic.<sup>30</sup> Still, the DFT analysis provides valuable insights into the structure of the MS-CPET transition state. This transition state is both the highest point along the proton reaction coordinate and the point where the electron transfers from  $\text{Flr(R)CO}_2^-$  to the oxidant (see above). The parallels between the DFT description of MS-CPET with the PT case are quite strong. Again, PT is farther along the reaction coordinate than would be expected from the Hammond postulate. Electronic reorganization within the fluorene lags behind the proton transfer.

One way to visualize MS-CPET in the Bernasconi PNS formalism is to represent the two electronic states as two More O’Ferrall–Jencks planes, as shown in Figure 3B. The bottom plane shows the nuclear reorganization to arrive at the transition state. Electron transfer for the MS-CPET reaction is shown by a “jump” from one plane to another, because it occurs instantaneously on the time scale of nuclear motions (the Franck–Condon principle).<sup>5a,30,31</sup> This takes the system to the upper plane where the nuclear reorganization is completed to form the product. This description is supported by the DFT calculations, which show that the NBO charge on the nitrogen atom of the oxidant sharply changes at the transition state, while the nuclear motions proceed smoothly before and after the transition state.

The late position of proton transfer along the reaction coordinate provides a rationale for the larger Brønsted  $\alpha$  upon changing the substituent than the oxidant. It is, however, more challenging to use this model to understand the small dependence of the rate constants on the reduction potential of oxidant ( $\alpha_{\text{ET}} = 0.2$ ). In a simple Marcus theory formalism, a small  $\alpha$  would normally indicate a strongly exoergic reaction, with  $-\Delta G^\circ$  approaching  $\lambda$ . This is not consistent with our estimates that MS-CPET is close to isoergic for the oxidation of  $\text{Flr(H)CO}_2^-$  with  $\text{FeCp}^*_2^+$ .<sup>12</sup> In addition, this explanation would require curvature of the  $\log(k_{\text{MS-CPET}})$  versus  $\log(K_{\text{eq-MS-CPET}})$  plots, which is not seen in Figure 1C. The TS for the MS-CPET is early only in the “electronic reorganization” coordinate, and this refers to  $\pi$  bond rearrangement in the developing fluorenyl radical, not electron transfer to the oxidant.

Understanding the small  $\alpha$  likely requires a more complete treatment, as reported recently by Sayfutyarova, Goldsmith, and Hammes-Schiffer.<sup>31</sup>

## CONCLUSIONS

Reported here is a detailed study of the fundamental properties of oxidative cleavage of C–H bonds, by multiple-site concerted proton–electron transfer (MS-CPET). This mechanism is a new addition to the arsenal of C–H bond functionalization reactions. Kinetic studies of a series of fluorenyl-benzoate substrates show that the second-order rate constants are much more sensitive to substituents on the benzoate than to changes in the reduction potential of the oxidant. This shows, surprisingly, that the  $k_{\text{MS-CPET}}$  values do not simply correlate with the reaction driving force ( $K_{\text{eq-MS-CPET}}$ ). The  $k_{\text{MS-CPET}}$  values vary much more dramatically when the  $K_{\text{eq}}$  is changed via the substituent (Brønsted  $\alpha_{\text{Fc}^+} = 0.6$ ) than when  $K_{\text{eq}}$  is changed with changes in the oxidant ( $\alpha_{\text{ET}} = 0.2$ ). Experimental and computational analyses indicate that these differences reflect a higher sensitivity to the  $\text{p}K_{\text{a}}$  of the base rather than the oxidizing power of the oxidant.

Computational experiments show that the MS-CPET transition state (TS) is later on the proton transfer reaction coordinate than would be expected from the Hammond postulate. In addition, the TS shows significantly more progress along the proton transfer coordinate than along a coordinate that describes electronic reorganization of the  $\pi$  bonding within the fluorenyl group. Similar features were observed in DFT analysis of intramolecular proton transfer (PT) within the same substrate. These studies indicate strong analogies between PT and MS-CPET, despite the latter reaction involving an outer-sphere electron transfer component. The description of these reactions is reminiscent of classical physical organic analyses of proton transfer from C–H bonds, such as Bernasconi's Principle of Nonperfect Synchronization.

The results reported here are, to our knowledge, the first examples of MS-CPET reactions that show such a clear differentiation between changes in the electron transfer and the proton transfer reaction coordinates. Because this is the only example that involves a C–H bond, we tentatively suggest that this asymmetry could be characteristic of MS-CPET of C–H bonds, just as it is for simple deprotonation of C–H versus N–H or O–H bonds. This asynchrony of the concerted  $\text{e}^-/\text{H}^+$  transfer should have implications for broader development of MS-CPET as a mechanism for C–H bond activation, for instance, in selectivity enforcement in synthetic reactions and enzymatic processes.

## EXPERIMENTAL SECTION

### General Considerations.

Reagents were typically purchased from Sigma-Aldrich, Alfa Aesar, or Acros and used as received. Solvents were obtained from Fisher, while deuterated solvents were from Cambridge Isotope Laboratories. Unless otherwise noted, experiments were performed in an  $\text{N}_2$ -filled glovebox using solvents that were sparged with argon and plumbed directly into the glovebox. Dimethylformamide was purified using a Glass Contour Solvent Purification System (Pure Process Technology, LLC, Nashua, NH). Acetonitrile was Burdick Jackson

low water grade and used without additional drying. All oxidants used were hexafluorophosphate ( $\text{PF}_6^-$ ) salts. Aminium<sup>27a</sup> and ferrocenium<sup>10d</sup> oxidants were prepared as described previously. NMR samples following MS-CPET reactions were prepared in an  $\text{N}_2$ -filled glovebox using degassed, deuterated solvents dried over activated 3 Å molecular sieves. NMR spectra were collected on Agilent DD2 400, 500, or 600 MHz spectrometers.

### DFT Calculations.

All calculations were performed using the *Gaussian 16* software package. All optimized geometries were confirmed to be local minima by vibrational analysis (no imaginary frequencies). Geometry optimizations and frequency calculations were performed at the B3LYP/def2-SVP or B3LYP/def2-TZVP level of theory. Cartesian coordinates of the optimized geometries of all species are given in the Supporting Information.

### Synthesis.

The carboxylic acids were generated by basic hydrolysis from the corresponding methyl ester. The methyl ester compounds were synthesized using a modified procedure from a previous report.<sup>22</sup> Fluorene (1.2 equiv), the appropriate methyl ester (1.0 equiv),  $\text{Pd}(\text{OAc})_2$  (2 mol %),  $\text{PCy}_3 \cdot \text{HBF}_4$  (4 mol %), and  $\text{Cs}_2\text{CO}_3$  (1.5 equiv) were added to a microwave vial that was equipped with a stir bar. The vial was evacuated and backfilled with  $\text{N}_2$  on a Schlenk line. DMF was taken directly from the solvent system inside the glovebox and syringed into the reaction vial. The reaction then was heated at 110 or 130 °C overnight (~16 h). The reaction was cooled to room temperature and diluted with 1 M HCl. The aqueous layer was extracted with  $\text{Et}_2\text{O}$  ( $3 \times 20$  mL), and then the organic layer was washed with 1 M HCl ( $2 \times 20$  mL),  $\text{H}_2\text{O}$  ( $2 \times 20$  mL), and brine (20 mL). The organic layer was dried over  $\text{MgSO}_4$  and solvent evaporated. The crude reaction mixture was purified on a silica gel column in 5% EtOAc:hexanes eluent. The methyl ester products generated via the above procedure were then treated with basic hydrolysis to yield the corresponding carboxylic acid. The isolated methyl ester was added to a degassed solution of ethanol and 3 M aqueous KOH. This solution was brought to reflux until a TLC revealed consumption of the methyl ester starting material (usually in about 15–30 min). The reaction mixture was cooled to room temperature and diluted with 1 M  $\text{HCl}_{\text{aq}}$  and washed with  $\text{Et}_2\text{O}$  to afford the carboxylic acids as white or off-white solids.

### Experimental $\text{p}K_{\text{a}}$ Measurements.

Measurements of the  $\text{p}K_{\text{a}}$ 's were performed in analogy to a previous report.<sup>10d</sup> In a typical experiment, a fluorenyl substrate was deprotonated with 1.0 equiv of 1,8-diazabicyclo[5.4.0]undec-7-ene (DBU) in an  $\text{N}_2$ -filled glovebox in  $\text{CD}_3\text{CN}$ . Next, 4-trifluoromethyl benzoic acid (TFBA) was added to the solution, the mixture was allowed to equilibrate, and  $^1\text{H}/^{19}\text{F}$  NMR spectra were measured to determine the chemical shifts of chosen hydrogen and fluorine atoms at equilibrium. The acid/base pair for each material is in rapid equilibrium, so only an averaged signal was observed for each. The chemical shifts of the averaged signal give the ratio of acid to carboxylate for that species, allowing determination of the quotient of the  $K_{\text{a}}$ 's of the two acids in solution. These data were used to construct a relative  $\text{p}K_{\text{a}}$  scale. The relative  $\text{p}K_{\text{a}}$  between TFBA and benzoic acid was also

measured, which gives the relative scale an absolute anchor because the  $pK_a$  of benzoic acid in MeCN is known.

### Kinetics.

Kinetic measurements were recorded on an OLIS-RSM 1000 single mixing stopped-flow spectrophotometer in Burdick & Jackson low water acetonitrile that was sparged with argon and plumbed directly into an N<sub>2</sub>-filled glovebox. Measurements at different temperatures were made on a TgK double mixing stopped-flow instrument at temperatures ranging from -40 to 15 °C.

## Supplementary Material

Refer to Web version on PubMed Central for supplementary material.

## ACKNOWLEDGMENTS

We acknowledge the U.S. NIH (2R01GM50422 to J.M.M.) for funding this work. We thank Zachary Goldsmith for computational advice.

## REFERENCES

- (1). (a)Hartwig JF Evolution of C–H bond functionalization from methane to methodology. *J. Am. Chem. Soc* 2016, 138, 2. [PubMed: 26566092] (b)Labinger JA; Bercaw JE Understanding and exploiting C–H bond activation. *Nature* 2002, 417, 507. [PubMed: 12037558] (c)He J; Wasa M; Chan KSL; Shao Q; Yu J-Q Palladium-Catalyzed Transformations of Alkyl C–H Bonds. *Chem. Rev* 2017, 117, 8754. [PubMed: 28697604] (d)Crabtree RH Alkane C–H activation and functionalization with homogeneous transition metal catalysts: A century of progress—A new millennium in prospect. *J. Chem. Soc., Dalton Trans* 2001, 2437.(e)Davies HML; Morton D Recent Advances in C–H Functionalization. *J. Org. Chem* 2016, 81, 343. [PubMed: 26769355] (f)Goldberg KI; Goldman AS Activation and Functionalization of CH Bonds; American Chemical Society: Washington, DC, 2004; Vol. 885.(g)Shul'pin GB Selectivity enhancement in functionalization of C–H bonds: A review. *Org. Biomol. Chem* 2010, 8, 4217. [PubMed: 20593075]
- (2). (a)Kochi JK Free Radicals; Wiley: New York, 1973; Vol. 2(b)Perkins M Free Radical Chemistry; Ellis Horwood: New York, 1994.(c)Burton G; Ingold KU Vitamin E: application of the principles of physical organic chemistry to the exploration of its structure and function. *Acc. Chem. Res* 1986, 19, 194.(d)Gutteridge JM; Halliwell B The measurement and mechanism of lipid peroxidation in biological systems. *Trends Biochem. Sci* 1990, 15, 129. [PubMed: 2187293] (e)Olah GA; Prakash GS Hydrocarbon Chemistry; John Wiley & Sons: New York, 1995.
- (3). Darcy JW; Koronkiewicz B; Parada GA; Mayer JM A Continuum of Proton-Coupled Electron Transfer Reactivity. *Acc. Chem. Res* 2018, 51, 2391. [PubMed: 30234963]
- (4). (a)Snider BB Manganese(III)-Based Oxidative Free-Radical Cyclizations. *Chem. Rev* 1996, 96, 339. [PubMed: 11848756] (b)Mayer JM Hydrogen atom abstraction by metal–oxo complexes: understanding the analogy with organic radical reactions. *Acc. Chem. Res* 1998, 31, 441.
- (5). (a)Reece SY; Nocera DG Proton-Coupled Electron Transfer in Biology: Results from Synergistic Studies in Natural and Model Systems. *Annu. Rev. Biochem* 2009, 78, 673. [PubMed: 19344235] (b)Jasniewski AJ; Que L Dioxygen Activation by Nonheme Diiron Enzymes: Diverse Dioxygen Adducts, High-Valent Intermediates, and Related Model Complexes. *Chem. Rev* 2018, 118, 2554. [PubMed: 29400961] (c)Solomon EI; Heppner DE; Johnston EM; Ginsbach JW; Cirera J; Qayyum M; Kieber-Emmons MT; Kjaergaard CH; Hadt RG; Tian L Copper Active Sites in Biology. *Chem. Rev* 2014, 114, 3659. [PubMed: 24588098]
- (6). (a)Rittle J; Green MT Cytochrome P450 Compound I: Capture, Characterization, and C-H Bond Activation Kinetics. *Science* 2010, 330, 933. [PubMed: 21071661] (b)Yosca TH; Rittle J; Krest

CM; Onderko EL; Silakov A; Calixto JC; Behan RK; Green MT Iron(IV)hydroxide pKa and the Role of Thiolate Ligation in C–H Bond Activation by Cytochrome P450. *Science* 2013, 342, 825. [PubMed: 24233717] (c)Groves JT Using push to get pull. *Nat. Chem* 2014, 6, 89. [PubMed: 24451580]

- (7). Warren JJ; Tronic TA; Mayer JM Thermochemistry of Proton-Coupled Electron Transfer Reagents and its Implications. *Chem. Rev* 2010, 110, 6961. [PubMed: 20925411]
- (8). Gentry EC; Knowles RR Synthetic Applications of Proton-Coupled Electron Transfer. *Acc. Chem. Res* 2016, 49, 1546. [PubMed: 27472068]
- (9). Keough JM; Jenson DL; Zuniga AN; Barry BA Proton Coupled Electron Transfer and Redox-Active Tyrosine Z in the Photosynthetic Oxygen-Evolving Complex. *J. Am. Chem. Soc* 2011, 133, 11084. [PubMed: 21714528]
- (10). (a)Markle TF; Rhile IJ; DiPasquale AG; Mayer JM Probing concerted proton–electron transfer in phenol–imidazoles. *Proc. Natl. Acad. Sci. U. S. A* 2008, 105, 8185. [PubMed: 18212121] (b)Markle TF; Mayer JM Concerted Proton–Electron Transfer in Pyridylphenols: The Importance of the Hydrogen Bond. *Angew. Chem., Int. Ed* 2008, 47, 738. (c)Markle TF; Rhile IJ; Mayer JM Kinetic effects of increased proton transfer distance on proton-coupled oxidations of phenol-amines. *J. Am. Chem. Soc* 2011, 133, 17341. [PubMed: 21919508] (d)Morris WD; Mayer JM Separating proton and electron transfer effects in three-component concerted proton-coupled electron transfer reactions. *J. Am. Chem. Soc* 2017, 139, 10312. [PubMed: 28671470] (e)Parada GA; Glover SD; Orthaber A; Hammarström L; Ott S Hydrogen Bonded Phenol-Quinolines with Highly Controlled Proton-Transfer Coordinate. *Eur. J. Org. Chem* 2016, 2016, 3365. (f)Wenger OS Proton-coupled electron transfer with photoexcited ruthenium(II), rhenium(I), and iridium(III) complexes. *Coord. Chem. Rev* 2015, 282–283, 150.
- (11). (a)Choi GJ; Zhu Q; Miller DC; Gu CJ; Knowles RR Catalytic alkylation of remote C–H bonds enabled by proton-coupled electron transfer. *Nature* 2016, 539, 268. [PubMed: 27732585] (b)Musacchio AJ; Lainhart BC; Zhang X; Naguib SG; Sherwood TC; Knowles RR Catalytic intermolecular hydroaminations of unactivated olefins with secondary alkyl amines. *Science* 2017, 355, 727. [PubMed: 28209894] (c)Zhu Q; Graff DE; Knowles RR Intermolecular Anti-Markovnikov Hydroamination of Unactivated Alkenes with Sulfonamides Enabled by Proton-Coupled Electron Transfer. *J. Am. Chem. Soc* 2018, 140, 741. [PubMed: 29268020] (d)Chu JCK; Rovis T Amide-directed photoredox-catalysed C–C bond formation at unactivated sp<sup>3</sup> C–H bonds. *Nature* 2016, 539, 272. [PubMed: 27732580] (e)Jia J; Ho YA; Bülow RF; Rueping M Brønsted Base Assisted Photoredox Catalysis: Proton Coupled Electron Transfer for Remote C–C Bond Formation via Amidyl Radicals. *Chem. - Eur. J* 2018, 24, 14054. [PubMed: 29939456] (f)Miller DC; Tarantino KT; Knowles RR Proton-Coupled Electron Transfer in Organic Synthesis: Fundamentals, Applications, and Opportunities. *Top. Curr. Chem* 2016, 374, 1.
- (12). Markle TF; Darcy JW; Mayer JM A new strategy to efficiently cleave and form C–H bonds using proton-coupled electron transfer. *Sci. Adv* 2018, 4, No. eaat5776. [PubMed: 30027119]
- (13). Shaik SS; Schlegel HB; Wolfe S *Theoretical Aspects of Physical Organic Chemistry*; Wiley: New York, 1992.
- (14). (a)Hanhart W; Ingold CK CXXXIX.—The nature of the alternating effect in carbon chains. Part XVIII. Mechanism of exhaustive methylation and its relation to anomalous hydrolysis. *J. Chem. Soc* 1927, 0, 997. (b)Letsinger RL; Schnizer AW; Bobko E Orientation in the Cleavage of 2-Methoxyoctane by Organoalkali Metal Compounds. *J. Am. Chem. Soc* 1951, 73, 5708. (c)Cram DJ; Greene FD; Depuy CH Studies in Stereochemistry. XXV. Eclipsing Effects in the *E*<sub>2</sub> Reaction. *J. Am. Chem. Soc* 1956, 78, 790. (d)Saunders WH; Williams RA Mechanisms of Elimination Reactions. II. Rates of Elimination from Some Substituted 2-Phenylethyl Bromides and 2-Phenylethyldimethylsulfonium Bromides. *J. Am. Chem. Soc* 1957, 79, 3712. (e)Saunders WH; Edison DH Mechanisms of Elimination Reactions. IV. Deuterium Isotope Effects in *E*<sub>2</sub> Reactions of Some 2-Phenylethyl Derivatives. *J. Am. Chem. Soc* 1960, 82, 138. (f)Bunnett JF The Mechanism of Bimolecular β-Elimination Reactions. *Angew. Chem., Int. Ed. Engl* 1962, 1, 225.
- (15). (a)Bordwell FG; Boyle WJ Acidities, Brønsted coefficients, and transition state structures for 1-arylnitroalkanes. *J. Am. Chem. Soc* 1972, 94, 3907. (b)Kresge A The nitroalkane anomaly. *Can. J. Chem* 1974, 52, 1897.
- (16). Bernasconi CF In *Advances in Physical Organic Chemistry*; Richard JP, Ed.; Academic Press: New York, 2010; Vol. 44, p 223.

- (17). (a) Jencks DA; Jencks WP The characterization of transition states by structure-reactivity coefficients. *J. Am. Chem. Soc* 1977, 99, 7948. (b) Jencks WP A primer for the Bema Hapothle. An empirical approach to the characterization of changing transition-state structures. *Chem. Rev* 1985, 85, 511. (c) Anslyn EV; Dougherty DA *Modern Physical Organic Chemistry*; University Science Books: CA, 2006.
- (18). (a) Bernasconi CF In *Advances in Physical Organic Chemistry*; Bethell D, Ed.; Academic Press: New York, 1992; Vol. 27, p 119. (b) Bernasconi CF The principle of nonperfect synchronization: more than a qualitative concept? *Acc. Chem. Res* 1992, 25, 9. (c) Bernasconi CF; Wenzel PJ Is there a transition-state imbalance for proton transfers in the gas phase? *Ab initio* study of the carbon-to-carbon proton transfer from acetaldehyde to its enolate ion. *J. Am. Chem. Soc* 1994, 116, 5405.
- (19). Grunwald E Structure-energy relations, reaction mechanism, and disparity of progress of concerted reaction events. *J. Am. Chem. Soc* 1985, 107, 125.
- (20). Guthrie JP Multidimensional Marcus theory: an analysis of concerted reactions. *J. Am. Chem. Soc* 1996, 118, 12878.
- (21). (a) Bím D; Maldonado-Domínguez M; Rulíšek L; Srnc M Beyond the classical thermodynamic contributions to hydrogen atom abstraction reactivity. *Proc. Natl. Acad. Sci. U. S. A* 2018, 115, No. E10287. [PubMed: 30254163] (b) Goetz MK; Anderson JS Experimental Evidence for pK<sub>a</sub>-Driven Asynchronicity in C–H Activation by a Terminal Co(III)–Oxo Complex. *J. Am. Chem. Soc* 2019, 141, 4051. [PubMed: 30739450] (c) Usharani D; Lacy DC; Borovik AS; Shaik S Dichotomous Hydrogen Atom Transfer vs Proton-Coupled Electron Transfer During Activation of X–H Bonds (X = C, N, O) by Nonheme Iron–Oxo Complexes of Variable Basicity. *J. Am. Chem. Soc* 2013, 135, 17090. [PubMed: 24124906] (d) Hodgkiss JM; Rosenthal J; Nocera DG The Relation between Hydrogen Atom Transfer and Proton-Coupled Electron Transfer in Model Systems In *Hydrogen-Transfer Reactions*; Hynes JT, Klinman JP, Limbach H-H, Schowen RL, Eds.; Wiley-VCH: New York, 2007; p 503.
- (22). Chen J-J; Onogi S; Hsieh Y-C; Hsiao C-C; Higashibayashi S; Sakurai H; Wu Y-T Palladium-Catalyzed Arylation of Methylene-Bridged Polyarenes: Synthesis and Structures of 9-Arylfluorene Derivatives. *Adv. Synth. Catal* 2012, 354, 1551.
- (23). Binstead R; Zuberbühler A; Jung B *Spectrum Software Associates*; Chapel Hill: NC, 2004.
- (24). Waidmann CR; Miller AJM; Ng C-WA; Scheuermann ML; Porter TR; Tronic TA; Mayer JM Using combinations of oxidants and bases as PCET reactants: thermochemical and practical considerations. *Energy Environ. Sci* 2012, 5, 7771.
- (25). Kosuke I *Acid-Base Dissociation Constants in Dipolar Aprotic Solvents*; Blackwell Scientific Publications: Oxford, 1990.
- (26). Amiri S; Reisenauer HP; Schreiner PR Electronic Effects on Atom Tunneling: Conformational Isomerization of Monomeric Para-Substituted Benzoic Acid Derivatives. *J. Am. Chem. Soc* 2010, 132, 15902. [PubMed: 20964409]
- (27). (a) Rhile IJ; Markle TF; Nagao H; DiPasquale AG; Lam OP; Lockwood MA; Rotter K; Mayer JM Concerted proton-electron transfer in the oxidation of hydrogen-bonded phenols. *J. Am. Chem. Soc* 2006, 128, 6075. [PubMed: 16669677] (b) Connelly NG; Geiger WE Chemical redox agents for organometallic chemistry. *Chem. Rev* 1996, 96, 877. [PubMed: 11848774]
- (28). Luo Y-R *Comprehensive Handbook of Chemical Bond Energies*; CRC Press: New York, 2007.
- (29). (a) Bernasconi CF; Wenzel PJ Transition State Imbalances in Gas Phase Proton Transfers. *Ab Initio* Study of the Carbon-to-Carbon Proton Transfer from the Protonated Acetaldehyde Cation to Acetaldehyde Enol. *J. Am. Chem. Soc* 1996, 118, 10494. (b) Bernasconi CF The principle of nonperfect synchronization: recent developments. *Adv. Phys. Org. Chem* 2010, 44, 223.
- (30). (a) Barbara PF; Meyer TJ; Ratner MA *Contemporary Issues in Electron Transfer Research*. *J. Phys. Chem* 1996, 100, 13148. (b) Hammes-Schiffer S; Stuchebrukhov AA Theory of Coupled Electron and Proton Transfer Reactions. *Chem. Rev* 2010, 110, 6939. [PubMed: 21049940]
- (31). Sayfutyarova ER; Goldsmith ZK; Hammes-Schiffer S Theoretical Study of C–H Bond Cleavage via Concerted Proton-Coupled Electron Transfer in Fluorenyl-Benzoates. *J. Am. Chem. Soc* 2018, 140, 15641. [PubMed: 30383371]
- (32). Bernasconi CF In *Advances in Physical Organic Chemistry*; Bethell D, Ed.; Academic Press: New York, 1992; Vol. 27, p 119.



- (33). Bourrez M; Steinmetz R; Ott S; Gloaguen F; Hammarström L Concerted proton-coupled electron transfer from a metal-hydride complex. *Nat. Chem* 2015, 7, 140.
- (34). Markle TF; Tronic TA; DiPasquale AG; Kaminsky W; Mayer JM Effect of basic site substituents on concerted proton–electron transfer in hydrogen-bonded pyridyl–phenols. *J. Phys. Chem. A* 2012, 116, 12249. [PubMed: 23176252]
- (35). Qiu G; Knowles RR Rate-Driving Force Relationships in the Multisite-PCET Activation of Ketones. *J. Am. Chem. Soc* 2019, 141, 2721–2730. [PubMed: 30665301]
- (36). (a)Manner VW Concerted Proton-Electron Transfer Reactions of Ruthenium and Cobalt Complexes: Studies on Distance Dependence and Spin Effects. Ph.D. Thesis; University of Washington, 2009.(b)Fecenko CJ; Thorp HH; Meyer TJ The Role of Free Energy Change in Coupled Electron–Proton Transfer. *J. Am. Chem. Soc* 2007, 129, 15098. [PubMed: 17999500] (c)Gunasekara T; Abramo GP; Hansen A; Neugebauer H; Bursch M; Grimme S; Norton JR TEMPO-Mediated Catalysis of the Sterically Hindered Hydrogen Atom Transfer Reaction between (C<sub>5</sub>Ph<sub>5</sub>)Cr(CO)<sub>3</sub>H and a Trityl Radical. *J. Am. Chem. Soc* 2019, 141, 1882. [PubMed: 30669845]
- (37). (a)Yao X; Gold MA; Pollack RM Transition State Imbalance in Proton Transfer from Phenyl Ring-Substituted 2-Tetralones to Acetate Ion. *J. Am. Chem. Soc* 1999, 121, 6220.(b)Bowden K; Hirani SIJ The acidity of weak carbon acids. Part 5. The kinetic acidities of substituted benzyl cyanides using substituted benzylamines as bases. *J. Chem. Soc., Perkin Trans. 2* 1990, 2, 1889. (c)Bell RP; Grainger S Brønsted exponents in the proton abstraction from derivatives of ethyl  $\alpha$ -benzylacetoacetate, 3-benzylpentane-2,4-dione, and benzylmalononitrile. *J. Chem. Soc., Perkin Trans. 2* 1976, 2, 1367.(d)Gandler JR; Bernasconi CF Kinetics of deprotonation of arylnitromethanes by benzoate ions in acetonitrile solution. Effect of equilibrium and nonequilibrium transition state solvation on intrinsic rate constants of proton transfers. *J. Am. Chem. Soc* 1992, 114, 631.(e)Keeffe JR; Morey J; Palmer CA; Lee JC The nitroalkane anomaly - solvent dependence. *J. Am. Chem. Soc* 1979, 101, 1295.(f)Barletta GL; Zou Y; Huskey WP; Jordan F Kinetics of C(2 $\alpha$ )-Proton Abstraction from 2-Benzylthiazolium Salts Leading to Enamines Relevant to Catalysis by Thiamin-Dependent Enzymes. *J. Am. Chem. Soc* 1997, 119, 2356.(g)Terrier F; Lelievre J; Chatrousse A-P; Farrell P Transition state imbalance in the ionization of nitro-aromatic hydrocarbons: 2,2',4,4'-tetrinitrodiphenylmethane and 2,4,4'-trinitrodiphenylmethane in aqueous dimethyl sulfoxide solutions. *J. Chem. Soc., Perkin Trans. 2* 1985, 2, 1479.
- (38). An alternative conceptual analysis would consider these reactions as proton transfers from the fluorenyl C–H bond to the benzoate concerted with electron transfer from the incipient carbanion to the oxidant. Analyzing via this approach would need to include the effects of substituents on both the pK<sub>a</sub> of the fluorine C–H bond and the reduction power of the carbanion. The CF<sub>3</sub> electron-withdrawing substituent makes the C–H more acidic and has an offsetting decrease in the reducing power of the carbanion. This balancing effect makes this a more challenging approach, and shows why separating out the  $\Delta G^\circ$  for just proton transfer is misleading. If changes in the fluorene acidity were a dominant effect in this reactivity, then we would predict a substituent effect opposite of the one observed: the CF<sub>3</sub> compound would be the most reactive as it would be the most acidic.<sup>a33</sup>
- (39). (a)Antonello S; Musumeci M; Wayner DDM; Maran F Electroreduction of Dialkyl Peroxides. Activation–Driving Force Relationships and Bond Dissociation Free Energies. *J. Am. Chem. Soc* 1997, 119, 9541.(b)Saveant JM A simple model for the kinetics of dissociative electron transfer in polar solvents. Application to the homogeneous and heterogeneous reduction of alkyl halides. *J. Am. Chem. Soc* 1987, 109, 6788.(c)Andrieux CP; Merz A; Saveant JM Dissociative electron transfer. Autocatalysis and kinetic characteristics of the electrochemical reductive cleavage of the carbon halogen bond in alkyl halides giving rise to stable radicals and carbanions. *J. Am. Chem. Soc* 1985, 107, 6097.
- (40). Kresge AJ Deviant Broensted relations. *J. Am. Chem. Soc* 1970, 92, 3210.
- (41). (a)Bernasconi CF; Wenzel PJ Carbon-to-Carbon Identity Proton Transfers from Propyne, Acetamide, Thioacetaldehyde, and Nitrosomethane to Their Respective Conjugate Anions in the Gas Phase. An *ab Initio* Study. *J. Org. Chem* 2001, 66, 968. [PubMed: 11430120] (b)Bernasconi CF; Wenzel PJ Carbon-to-carbon identity proton transfer from allene, ketene, ketenimine, and

thioetene to their respective conjugate anions in the gas phase. An *ab initio* study. J. Am. Chem. Soc 2001, 123, 7146. [PubMed: 11459495]

- (42). Marcus RA Unusual slopes of free energy plots in kinetics. J. Am. Chem. Soc 1969, 91, 7224.
- (43). Guthrie JP Prediction of the Rate Constants for Proton Abstraction from Carbon Acids, Using a Simple Model and Multidimensional Marcus Theory. J. Am. Chem. Soc 1997, 119, 1151.
- (44). Jencks WP General acid-base catalysis of complex reactions in water. Chem. Rev 1972, 72, 705.

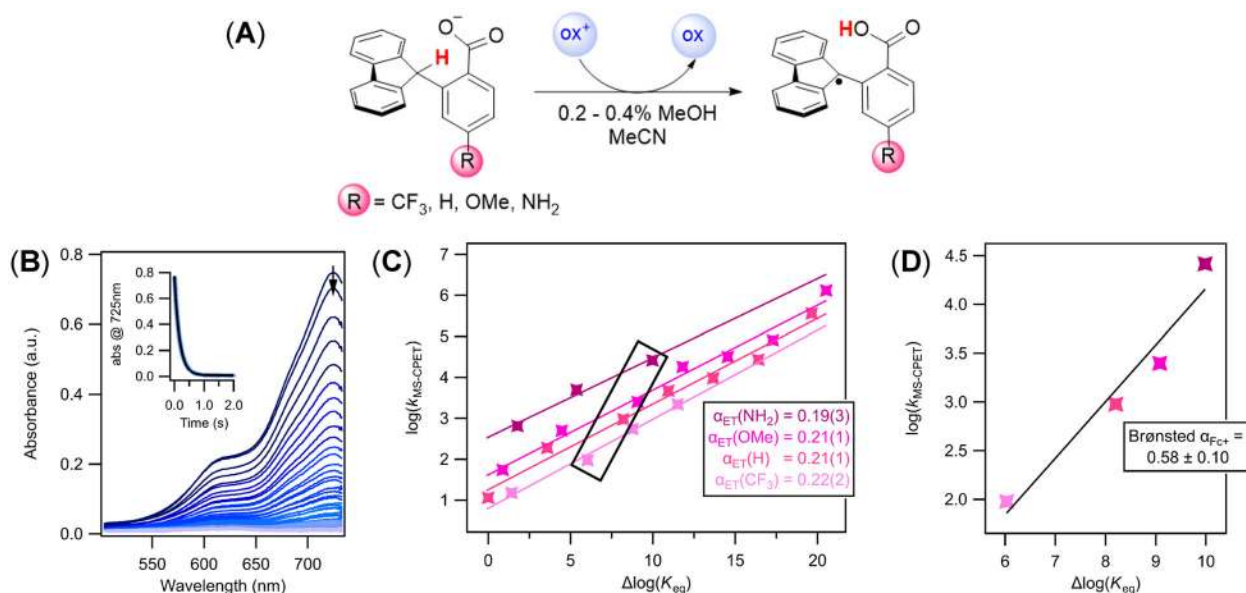


**Figure 1.**

(A) General reaction scheme for the oxidation of  $\text{Flr}(\text{R})\text{CO}_2^-$  substrates. Reactions were performed with an excess of carboxylate, generated in situ with TBAOH (as a solution in MeOH). Absorbance spectra were monitored on a stopped-flow following the disappearance of the colored aminium and ferrocenium oxidants. (B) Representative absorbance versus time data set monitoring the reaction of  $\text{N}(\text{Ar}_{\text{OMe}})_3^{*+}$  with  $\text{Flr}(\text{OMe})\text{CO}_2^-$ . The inset shows the absorbance at the  $\lambda_{\text{max}}$  of the oxidant, 752 nm, versus time, and the fit to an exponential function using SpecFit global fitting software. (C) Plot of the logarithm of the MS-CPET rate constants ( $k_{\text{MS-CPET}} = k_2/2$ ) versus changes in driving force for all substrates over a range of oxidants.  $\Delta\log(K_{\text{eq}}) = -\Delta\Delta G^\circ_{\text{rxn}}/2.303RT$  and  $\Delta\Delta G^\circ_{\text{rxn}} = \Delta\text{BDFE}_{\text{CH}}(\text{CO}_2\text{H}) - 1.37\Delta\text{p}K_{\text{a}}(\text{CO}_2\text{H}) - 23.06E_{\text{ox}}$  (see text and Scheme 2). The  $\Delta\log(K_{\text{eq}})$  for the reaction of the  $\text{R} = \text{H}$  compound with  $\text{FeCp}^*_2^+$  has been set equal to zero,<sup>12</sup> and all other values are relative to that based on changes in  $\text{BDFE}_{\text{CH}}$  and  $\text{p}K_{\text{a,COOH}}$  (see the Supporting Information for all values). Uncertainty in the last decimal is shown in parentheses. (D) Plot of MS-CPET rate constants versus changes in driving force for the four substrates with a single oxidant ( $\text{FeCp}_2^+$ ).

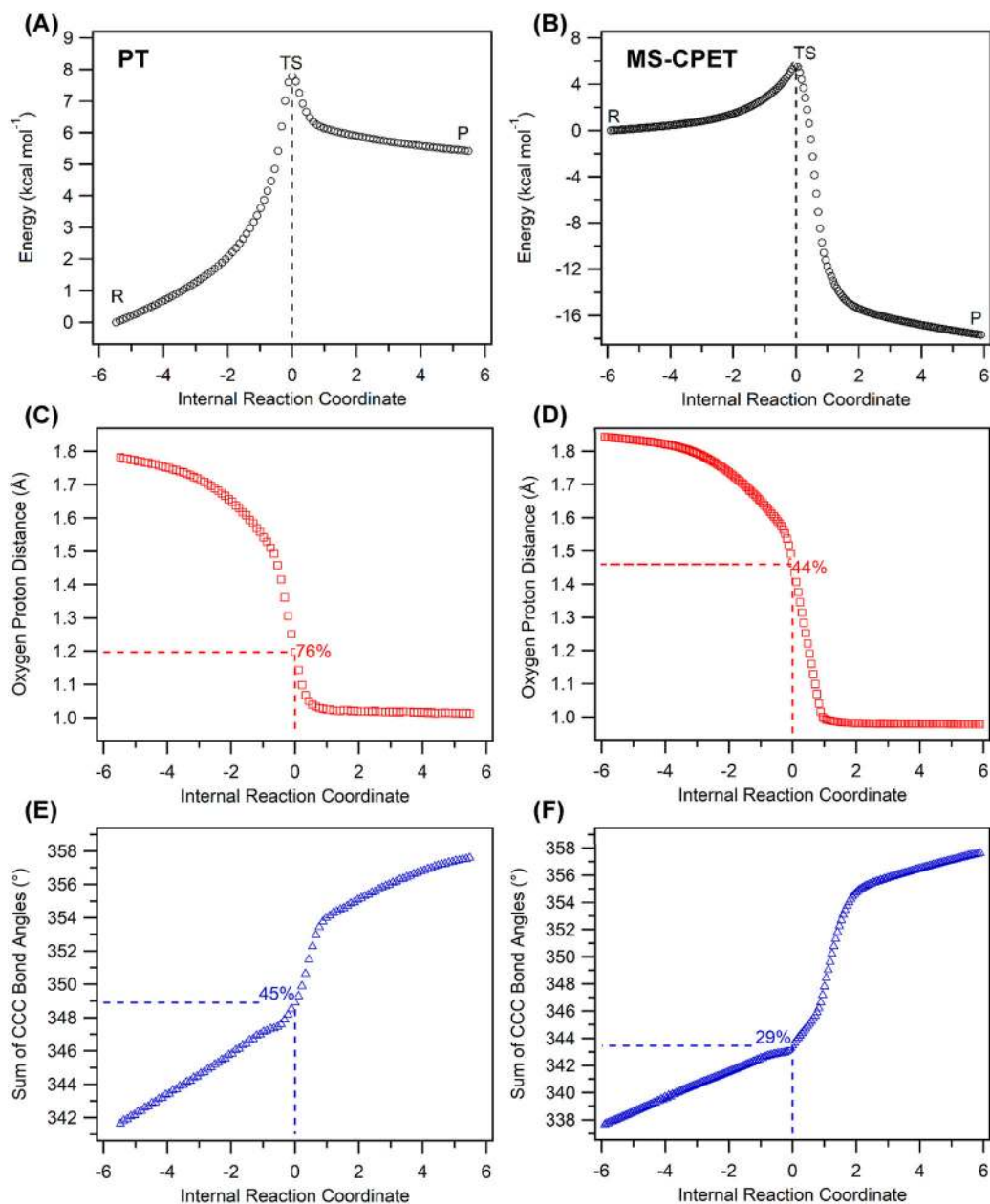


**Figure 2.**

Comparison of the DFT-computed internal reaction coordinates and transition states for intramolecular PT in  $\text{Flr}(\text{H})\text{CO}_2^-$  (A, C, and E) and for the MS-CPET reaction of  $\text{Flr}(\text{H})\text{CO}_2^-$  and  $\text{N}(\text{Ar}_B)_3^{*+}$  (B, D, and F). (A and B) The transition state occurs at  $x = 0$  along the reaction coordinate. Proceeding to negative values along the  $x$ -axis leads toward reactants, while proceeding to positive values leads to products. Black “O” show potential energy ( $\Delta E$ ) along the reaction coordinate. (C and D) Red “□” show the distance between the fluorenyl proton and the carboxylate oxygen along the reaction coordinate, which is a measure of proton transfer. For intramolecular PT, the fluorenyl proton has proceeded 76% toward the carboxylate oxygen. For MS-CPET, the fluorenyl proton has proceeded 44% toward the carboxylate oxygen. (E and F) Blue “Δ” show the sum of the CCC bond angles

along the fluorenyl carbon along the reaction coordinate, which is a measure of electronic reorganization. For intramolecular PT, the sum of the fluorenyl CCC bond angles has proceeded 45% toward the final geometry. For MS-CPET, the sum of the fluorenyl CCC bond angles has proceeded 29% toward the final geometry.

Author Manuscript

Author Manuscript

Author Manuscript

Author Manuscript

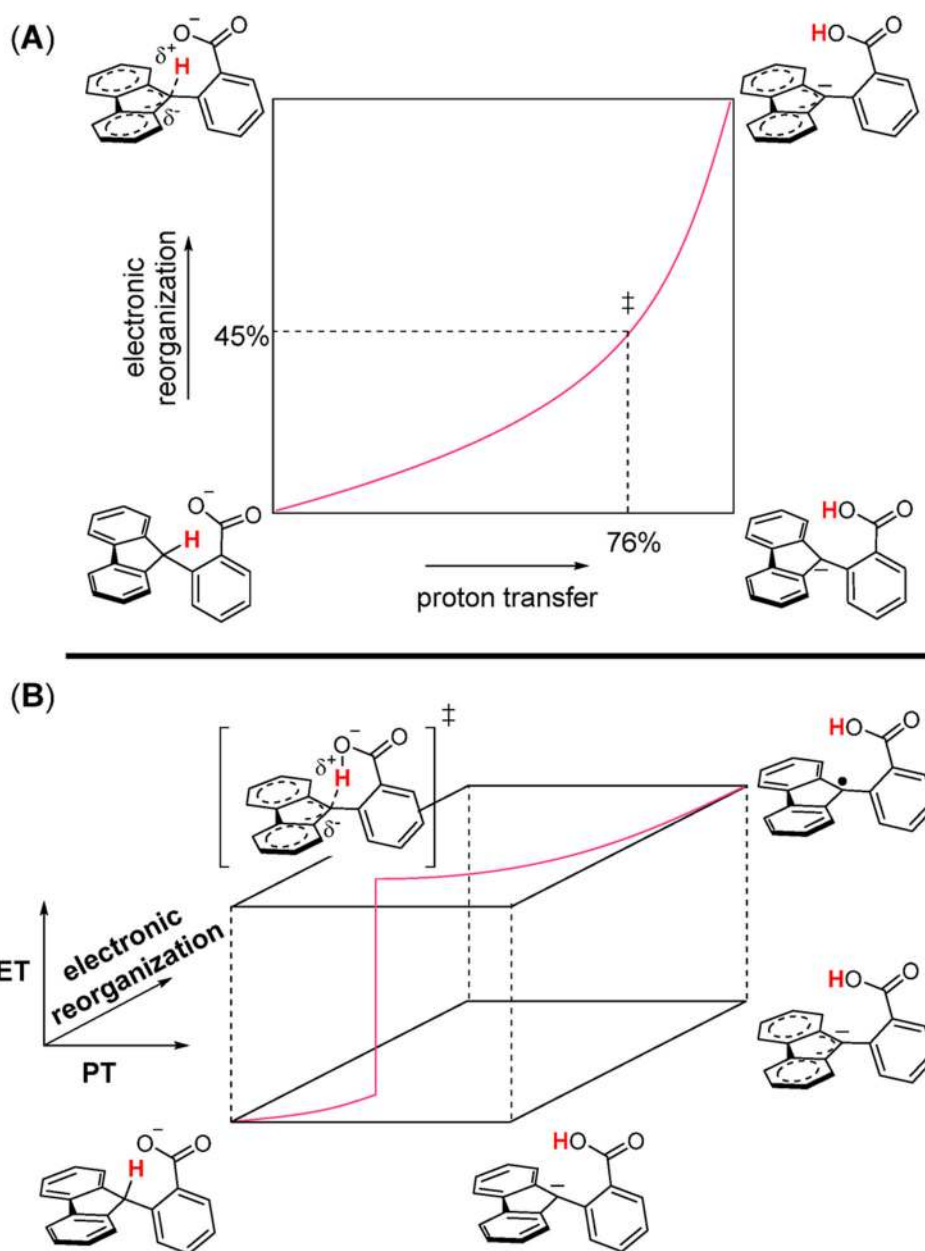
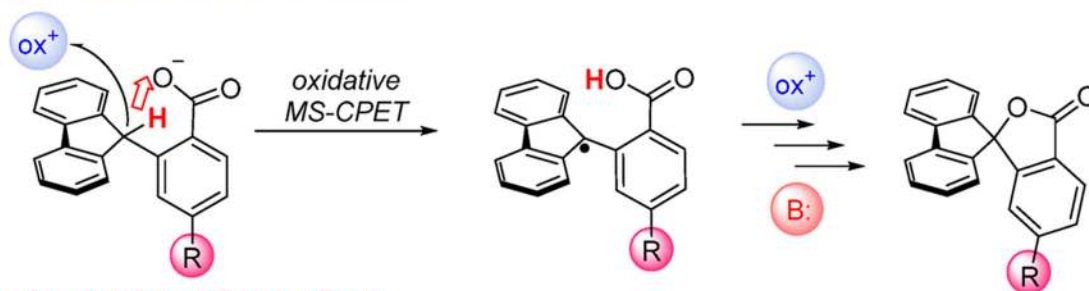


**Figure 3.** (A) A More O'Ferrall-Jencks plot for intramolecular proton transfer in  $\text{Flr}(\text{H})\text{CO}_2^-$ . The progress of the proton transfer and electronic reorganization at the transition state ( $\ddagger$ ) are noted with dashed lines. (B) A double More O'Ferrall-Jencks plot for the MS-CPET reaction of  $\text{Flr}(\text{H})\text{CO}_2^-$  with an outer-sphere oxidant. As in part (A), each of the two horizontal planes illustrates the progress in the proton transfer coordinate and in the electronic reorganization coordinate. The jump from the bottom to the top plane represents the electron transfer to the oxidant, an essentially instantaneous step that takes the system from one electronic state to another.

Modulate the electron transfer driving force  
by changing the  $E_{1/2}$  of the external oxidant



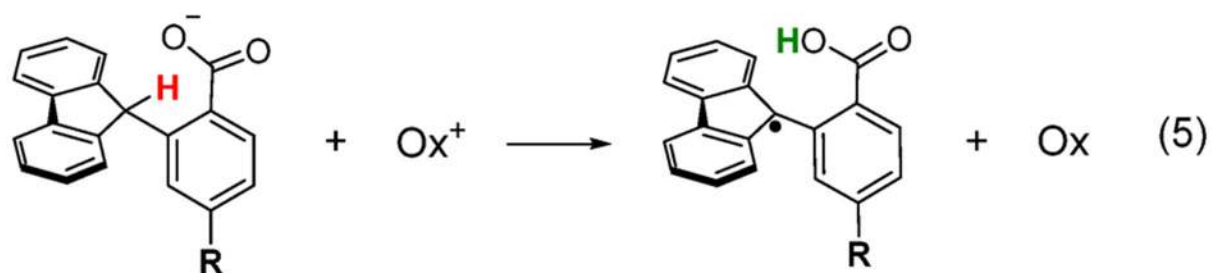
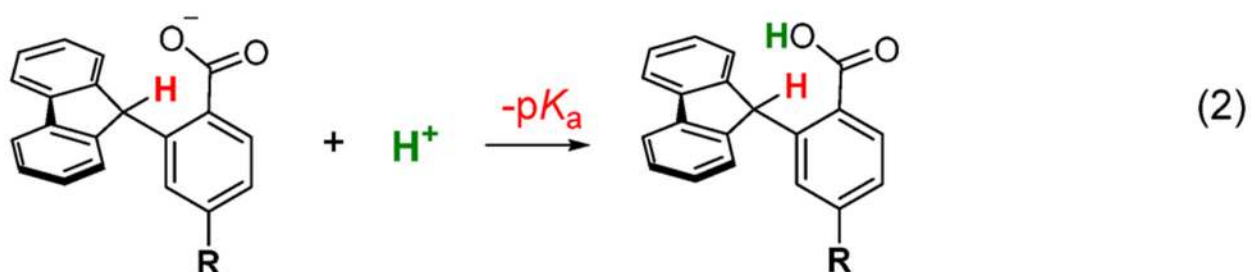
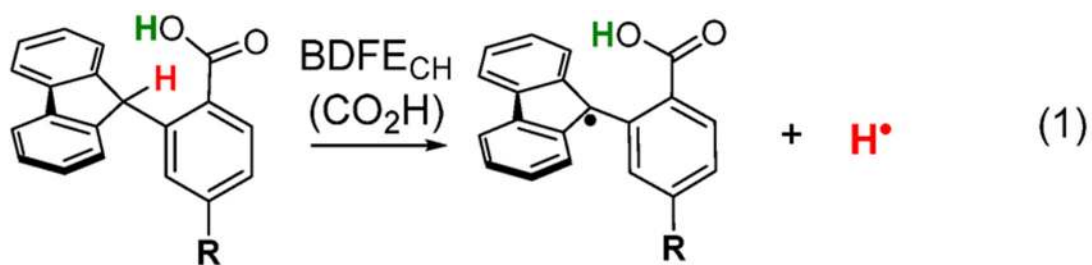
Modulate the proton transfer coordinate  
by changing the  $pK_a$  of the internal carboxylate



**Scheme 1. MS-CPET at Fluorenyl-benzoates Flr(R)CO**

$2^-$ , R = CF<sub>3</sub>, H, OMe, NH<sub>2</sub><sup>a</sup>

<sup>a</sup>The driving forces for proton and electron transfer can be modulated by changing the  $pK_a$  of the internal base and the  $E_{1/2}$  of the external oxidant, respectively. Oxidation leads to the formation of the carbon centered radical, which is subsequently converted to the corresponding lactone.



Scheme 2. Thermochemical Cycle To Determine the Relative Free Energies of MS-CPET Oxidation of the Fluorenyl C-H Bonds



Table 1.

Second-Order Rate Constants for the Reactions of Carboxylates with Oxidants of Varying Potential (Eox) in MeCN<sup>d</sup>

entry	oxidant <sup>b</sup>	$E_{ox}$ (V) <sup>c</sup>	$k_1(\text{NH}_2)\text{CO}_2^- k_2$ ( $\text{M}^{-1} \text{s}^{-1}$ ) <sup>d</sup>	$k_1(\text{OMe})\text{CO}_2^- k_2$ ( $\text{M}^{-1} \text{s}^{-1}$ ) <sup>d</sup>	$k_1(\text{H})\text{CO}_2^- k_2$ ( $\text{M}^{-1} \text{s}^{-1}$ ) <sup>d,e</sup>	$k_1(\text{CF}_3)\text{CO}_2^- k_2$ ( $\text{M}^{-1} \text{s}^{-1}$ ) <sup>d</sup>
1	N(Ar <sub>Bz</sub> ) <sub>3</sub> <sup>++</sup>	0.67	nd	$2.6 \times 10^6$	$7.2 \times 10^5$	nd
2	N(Ar <sub>OMe</sub> ) <sub>3</sub> <sup>++</sup>	0.48	nd	$1.6 \times 10^5$	$5.4 \times 10^4$	nd
3	N(Ar <sub>OMe</sub> ) <sub>2</sub> (Ar <sub>Bz</sub> ) <sup>++</sup>	0.32	nd	$6.3 \times 10^4$	$1.9 \times 10^4$	$4.4 \times 10^3$
4	N(Ar <sub>OMe</sub> ) <sub>3</sub> <sup>++</sup>	0.16	nd	$3.6 \times 10^4$	$9.5 \times 10^3$	$1.1 \times 10^3$
5	FeCp <sub>2</sub> <sup>+</sup>	0.00	$5.2 \times 10^4$	$5.0 \times 10^3$	$1.9 \times 10^3$	$1.9 \times 10^2$
6	FeCp* <sup>+</sup>	-0.27	$1.0 \times 10^4$	$1.0 \times 10^3$	$3.8 \times 10^2$	$3.0 \times 10^1$
7	FeCp* <sub>2</sub> <sup>+</sup>	-0.48	$1.3 \times 10^3$	$1.1 \times 10^2$	$2.3 \times 10^1$	nd

<sup>a</sup> Carboxylates generated in situ from carboxylic acids using 0.9 equiv of TBAOH (1 M in CH<sub>3</sub>OH); nd = not determined.

<sup>b</sup> ArX = *p*-C<sub>6</sub>H<sub>4</sub>-X; Cp = η<sup>5</sup>-C<sub>5</sub>H<sub>5</sub>; Cp\* = η<sup>5</sup>-C<sub>5</sub>Me<sub>5</sub>; all oxidants are PF<sub>6</sub><sup>-</sup> salts.

<sup>c</sup>  $E_{1/2}$  versus FeCp<sub>2</sub><sup>+0</sup> in MeCN.

<sup>d</sup> In MeCN with 0.2 vol % MeOH (NAr<sub>3</sub><sup>++</sup>) or 0.4 vol % MeOH (Fe<sup>+</sup>); uncertainties in  $k_2$  ca. ±10%.

<sup>e</sup> Data previously reported in ref 12.

**Table 2.**Activation Parameters for Oxidations of Flr(R)CO<sub>2</sub><sup>-</sup> by N•+(ArOMe)<sub>3</sub><sup>a</sup>

compound	$\Delta H^\ddagger$	$\Delta S^\ddagger$
Flr(OMe)CO <sub>2</sub> <sup>-b</sup>	14.4 ± 0.1	11.8 ± 0.5
Flr(H)CO <sub>2</sub> <sup>-b</sup>	15.2 ± 0.3	11.6 ± 1.0
Flr(CF <sub>3</sub> )CO <sub>2</sub> <sup>-c</sup>	16.3 ± 0.2	12.2 ± 0.8

<sup>a</sup>See Supporting Information section 3.4.  $\Delta H^\ddagger$  in kcal mol<sup>-1</sup>;  $\Delta S^\ddagger$  in cal K<sup>-1</sup> mol<sup>-1</sup>. Uncertainties are one standard deviation (1 $\sigma$ ).<sup>b</sup>Based on *k*<sub>MS-CPET</sub> from -40 to 15 °C.<sup>c</sup>Based on *k*<sub>MS-CPET</sub> from -20 to 15 °C.

Author Manuscript

Author Manuscript

Author Manuscript

Author Manuscript

**Table 3.**

Changes in Thermodynamic Parameters with Substituent for Substituted Fluorenyl-benzoates, from Experiment and DFT Calculations<sup>a</sup>

R	pK <sub>a</sub> (CO <sub>2</sub> H) expt	ΔpK <sub>a</sub> (CO <sub>2</sub> H) expt	ΔBDFE <sub>CH</sub> (CO <sub>2</sub> ) <sup>b</sup> (kcal mol <sup>-1</sup> )
NH <sub>2</sub>	22.0	+0.8	-0.06
OMe	21.5	+0.3	0.22
H	21.2	0	0
CF <sub>3</sub>	20.3	-0.9	0.83

<sup>a</sup>Relative values are versus the R = H compound.

<sup>b</sup>Differences in the DFT-computed bond dissociation free energies (BDFEs) for the carboxylate fluorenyl C–H bond (B3LYP/def2-TZVP with PCM = MeCN).